6 Rotationally symmetrical surfaces: Spherical Surfaces

In this Section we will present the results of measuring radii of curvature and surface topographies obtained with samples of a rotationally symmetrical geometry, which have been chosen to be spherical surfaces. Section 6.1 depicts the main features of the surfaces being tested; the selection of the samples and the consideration of spherical geometries as representative of rotationally symmetrical surfaces will also be explained and justified throughout this section. Six different spherical surfaces, grouped in pairs with nominally identical radii of curvature, will be measured at three different distances from the Ronchi ruling. Consequently only three different nominal radii of curvature will be measured.

After explaining the selection procedure of the samples, Section 6.2 presents a typical measurement process, following the data processing steps described in Section

4.2. Image captions for many of the steps involved in the measurement process will be presented for one of the sample surfaces at a given distance to the Ronchi ruling, in order to provide the reader with a complete view of a typical measurement process using our approach to Ronchi deflectometry. Confidence intervals, sampled areas, standard deviations of all the fitted values and residuals from the best-fit measured sphere will be provided for this measurement, and conclusions will be drawn on the usefulness of microstepping techniques. A final validation step will be performed by comparing the measured radius of curvature values using the Ronchi test with high precision radioscopic measurements.

However, as our setup is capable of measuring rotationally symmetrical surfaces and building their surface topographies, its ability to measure topographies of rotationally symmetrical surfaces will be presented to the reader. We will furthermore take advantage of the simple geometry of the samples to perform an analysis of some of the characteristics that may affect the performance of the measurement technique, which could be useful when interpreting some of the results obtained when testing more complex surfaces. In Section 6.3, radius of curvature measurements and topographies for the six samples involved are presented, allowing some insight into the measuring technique's capabilities.

6.1 Sample surfaces

Many rotationally symmetrical surfaces with optical quality may be found today in real-world applications. As they are easily manufactured from a single curve under rotation, spherical and aspherical surfaces are becoming commonplace in many fields close to optics. The paraboloid and hyperboloid shapes used in automobile light reflectors are just one example of a geometry increasingly present in today's technology.

Spherical and aspherical surfaces are the rotationally symmetrical geometries that may be found in this kind of sample. In fact, it is well known that both kinds of surfaces may be expressed as a single equation using cylindrical coordinates through

$$z = \frac{a\frac{r}{R}}{1+\sqrt{1-\left(a\frac{r}{R}\right)^2}} \qquad (6.1.1)$$

where *a* is the conic constant, *r* the distance polar coordinate on XY plane and *R* the radius of curvature of the sphere tangent to the surface at the origin. For spherical surfaces, *a* equals unity.

The measurement of such kinds of surfaces using the Ronchi test has already been studied [Cornejo 1970] [Malacara 1974], although the samples, interpretation and experimental setup of the Ronchi test in those references is quite different from the one we use, as, for instance, a single ronchigram is used in order to test telescope primary mirrors. Besides, no surface topography is provided, as obviously neither powerful numerical computing tools nor CCD devices were available in the seventies, and because these techniques mainly focus on the detection of manufacturing flaws on the surface from the observation of deformations of the shadows in the ronchigram.

In our approach to Ronchi deflectometry, no fundamental difference exists between spherical and aspherical surfaces in data processing or data acquisition procedures. The main difference would lie in the fitting procedures used for the measurement of the radius of curvature, where the conic constant of the section of the considered surface along the X and Y directions needs to be taken into account in the case of aspherical surfaces, as, for instance, in two-dimensional fitting procedures the $N_x(x_S)$ and $N_y(y_S)$ plots will not follow a single line and obviously no linear regression procedure would be possible. However, simply including an additional parameter related to the conic constant in the two-dimensional fitting procedures would yield the values for both the radius of curvature and the conic constant, in a very similar way to the measurement of radius of curvature through two-dimensional fitting (linear regression) in spherical surfaces. Three-dimensional curve-fitting procedures including the conic constant would also be valid in the case of aspherical surfaces.

Because of these similarities, and also because of their availability, only spherical concave surfaces have been used as samples in the present work. This means that only one parameter (the radius of curvature) is allowed in both the two-dimensional and three-dimensional fitting procedures, apart from the centering terms needed in order to position the surface properly. Aspherical surfaces are also easily measured in our setup, but in this section our aim is to provide a consistent description and validation of our measuring technique rather than to perform measurements for all

the possible types of rotationally symmetrical surfaces available. The validation of the measurement technique will be performed in Section 6.2.3 by comparing the radius of curvature obtained with the techniques described in this work with the one obtained using a Möller-Wedel Measuring Combination V, in its high precision radioscope configuration. This validation will be further confirmed in Section 6.3 when comparing the radii of curvature of the surface topographies of each spherical surface with the corresponding reference measurements, at three different distances from the Ronchi ruling to the surface.

It is important to note that this comparison of Ronchi measurements with radioscope data will still be available when measuring toroidal surfaces in Section 7, but the accuracy of the measurements will be greatly reduced, as the radioscope is intended to measure radii of curvature of spherical surfaces and for toroidal surfaces only a lower accuracy estimate of the radius of curvature will be possible. Section 6.2.3 and Section 6.3 will thus show whether our setup is suitably calibrated by comparing accurate experimental measurements with the ones obtained using the Ronchi test technique.

As explained in Section 4.1.3, the samples tested will be concave surfaces of common ophthalmic lenses, whose convex surface has been made optically inactive by grinding it and painting it using matt black paint. This kind of sample was chosen because of its ready availability and because it is able to provide both rotationally and non-rotationally symmetrical surfaces[1]. The ease of obtaining a variety of radius of curvature values and the importance of the ophthalmic lens testing industry were also taken into account when making this choice.

Six different surfaces corresponding to three nominally different ophthalmic lenses will be tested. This means that three sets of two nominally identical surfaces will be tested, but due to the different accuracy of our method when compared to the procedures commonly used in the ophthalmic industry (which, as is well known, classifies lenses in 0.25 dioptres back vertex power steps) the measurements of curvature radii of nominally identical surfaces performed in our setup may differ slightly.

[1]Common ophthalmic lenses are manufactured with its concave surface spherical or toroidal, if the lens is a spherical or toric one respectively. Aspherical and progressive surfaces are usually used in the convex surfaces of the lenses for design reasons; however, concave aspherical and progressive surfaces are also commonplace in the ophthalmic industry, as they are used in the glass moulds used in organic lens manufacturing [Caum 1997].

These test surfaces will be named after the nominal back vertex power of the lenses they belong to, as shown in Table 6.1.1. The values of the radius of curvature for each surface obtained using the Möller-Wedel high precision radioscope are also listed in Table 6.1.1.

Table 6.1.1: Name, back vertex power (BVP), radius of curvature obtained using the Möller-Wedel high precision radioscope (R) and d_R distances to the Ronchi ruling (P1, P2 and P3) of the spherical surfaces tested.

Name	B.V.P.(D)	R(mm)	P1(mm)	P2(mm)	P3(mm)
P175A	1.75	149.7	171.2	177.3	183.5
P175B	1.75	149.8	171.2	177.3	183.5
P200A	2.00	159.3	181.2	187.2	192.9
P200B	2.00	159.4	181.1	187.1	192.8
P275A	2.75	160.2	180.8	185.7	193.3
P275B	2.75	161.0	180.8	185.7	193.3

These spherical surfaces will provide us with a valuable tool for investigating some properties of the measurements performed using our approach to Ronchi deflectometry. One of our main concerns was how slope measurements relied on distance measurements, so we intended to test the stability of the measurement by testing the same sample at three different distances from the Ronchi test to the surface. This distance has been called d_R throughout previous sections. The positions to test were selected under the criterion that the number of fringes in the test should lie between 7-8 bright lines at small d_R distances and 12-14 bright lines at longer d_R distances. The intermediate distance usually has ten bright lines. Such a number of bright fringes was considered in order to keep computation time under reasonable values once the microstepping procedures are applied, as explained in Section 5.3.2. The drawback of such a criterion is the relatively small increment in d_R from the longest to the shortest distance. More lines (and subsequently relatively bigger z increments) could be considered if microstepping techniques were not applied. Once the particular application to which the measurement technique was to be applied is known, a compromise combining accuracy, sampling, distance from the Ronchi ruling to the

surface and computation time needs to be considered. The three d_R distances for each surface, selected going by the aforementioned criterion are listed in Table 6.1.1, and named P1, P2 and P3.

The radius of curvature values of the surfaces selected need further comment, because of their similarity. Longer radii of curvature violate one of the conditions we assumed when developing the propagation equations: namely, the distance from the Ronchi ruling to the surface was assumed to be d_R>R, that is, we assumed the experimental setup to work “out of focus”. Longer radii of curvature would push us to work “in focus” in our current experimental setup, which merely would need some sign rewriting of the propagation equations and could be adequately performed in our experimental setup, in the same way as the usual “out of focus” measurements. Radii of curvature shorter than the ones presented in Table 6.1.1, which are easily found in meniscus negative lenses, can be measured “out of focus” following the described procedure, but unfortunately cannot be properly measured under the working conditions of our experimental setup, as the minimum distance from the lens vertex to the Ronchi ruling is mechanically limited to d_R^{MIN}=112.6mm. All the equations and analysis performed in Sections 3.3 and 4.2 used for the calculation of the slope and position of the reflected ray impinging on the Ronchi ruling assume d_R>R, but an additional problem caused by the great d_R^{MIN} distance of our current experimental setup appears: small radii of curvature imply large incident beam slopes which, combined with the apertures of the produce large reductions in the measured area. Just as an instance, the CCD objective is only 50mm in diameter and is placed at least d_R^{MIN}=112.6mm away from the sample surface. Future improvements in the experimental setup will involve removing this basic limitation by decreasing this d_R distance as far as possible and increasing the diameter of the apertures of the system.

6.2 Typical measurement example

The full measurement process from the initial ronchigrams to the final surface topography and radius of curvature measurements will now be presented step by step. One of the sample surfaces in Table 6.1.1 at one particular distance from the Ronchi ruling to the surface will be selected in order to illustrate a typical measurement process fully. Measurement processes for any of the other samples or positions only differ from the one presented here in some of the numerical values obtained and in the number of bright lines present in the ronchigram. Image captions and graphs of the intermediate steps of the data processing will be presented in Section 6.2.1. The error analysis and tolerances of the measurement of the radius of curvature and the centering parameters of the surface will be presented in Section 6.2.2, while in Section 6.2.3 the measured results of the radius of curvature will be compared with the high precision radioscopic measurements used as reference values.

The results obtained when applying microstepping procedures will be shown next to the ones obtained without applying them, in order to illustrate the improvements in the measuring process entailed by the technique proposed in Section 5.3. However, due to the similarity of much of the data involved, the whole set of twenty original experimental measurements needed to perform a complete microstepping procedure will not be presented, as these are a family of ronchigrams which only differ in a T/10 displacement of the ruling in each direction. Only the first pair of original ronchigrams will be presented, as the remaining ones are just versions of this pair with their lines slightly displaced. In order to provide intermediate comparisons between microstepped and non-microstepped procedures, which are different from just the final radius of curvature or topographies obtained, some additional remarks and figures will be provided in the text presenting the differences between both procedures. It is emphasized that data acquisition for *both* microstepped and non-microstepped procedures has been carried out for *each* of the samples and positions, although obviously the data in the non-microstepped pair of ronchigrams is equivalent to the data in the first pair of ronchigrams of the series of twenty ronchigrams recorded when performing microstepping techniques, as the same surface is placed at the same d_R distance. The complete data processing algorithms have also been carried out both for microstepped and non-microstepped data, in the three positions of each sample,

yielding conclusions fully equivalent to the ones that will be obtained in the case of this typical measurement example.

Intermediate graphs of the slope of the wavefront reflected on the surface against position will be presented at the Ronchi ruling plane ($u(x_R)$ and $v(y_R)$), and at the tangent plane to the sample surface ($u(x_S)$ and $v(y_S)$). On the plane tangent to the sample surface at its vertex, graphs of the measured components of the local normal to the surface against position ($N_X(x_S)$ and $N_Y(y_S)$), are also presented. The comparison of the fitted values of the $u(x_S)$ and $N_X(x_S)$ plots, and of the $v(y_S)$ and $N_Y(y_S)$ plots show how, under our experimental conditions, that is, with the light source staying close to the center of curvature of the surface, confusing the slope of the reflected wavefront with the corresponding component of the local normal has negligible effects. This will be used to justify our previous assumption of ray-tracing the measured slopes and positions on the Ronchi plane to the plane tangent to the surface at its vertex, instead of ray-tracing them to the real surface, as under the experimental conditions of light source close to the center of curvature of the surface, the angular error introduced in this assumption is much smaller than the one introduced when confusing the $u(x_S)$ and $N_X(x_S)$ plots, or the $v(y_S)$ and $N_Y(y_S)$ plots.

6.2.1.- Measurement of sample P175A at position P1.

As the experimental and data processing procedures are equivalent in each of the samples and positions, the first one in Table 6.1.1 was arbitrarily selected, that is, sample P175A with a d_R distance of 171.2mm.

Prior to obtaining the ronchigrams to be used as data in order to start data processing, a previous step is performed in order to establish an absolute origin for the position of the lines on the ruling. It should be stressed that a “marked” line in the Ronchi test was used as a reference in order to set an absolute value for the line positions, as the relative distances between lines were known from the period of the ruling. This line was then displaced a whole number of periods through the Oriel Mike® encoder motors to take it outside the camera’s field of view. These reference ronchigrams are presented in Fig 6.2.1. The “mark” is easily seen when Fig.6.2.1 is compared to Fig.6.2.2, as obviously two bright lines have been hidden. The lines used as a reference are the first bright line above the mark, when lines are along the X axis (ronchigram with horizontal lines) and the first bright line on the left of the mark when lines are placed along the Y axis (ronchigram with vertical lines).

Fig. 6.2.1: Reference ronchigrams showing the “mark” on the ruling; two bright lines are missing when compared to Fig. 6.2.2. (a) Ruling lines along the X axis: the reference line is the first one above the “mark”; (b) Ruling lines along the Y axis: the reference line is the first one on the left of the “mark”.

(a) (b)

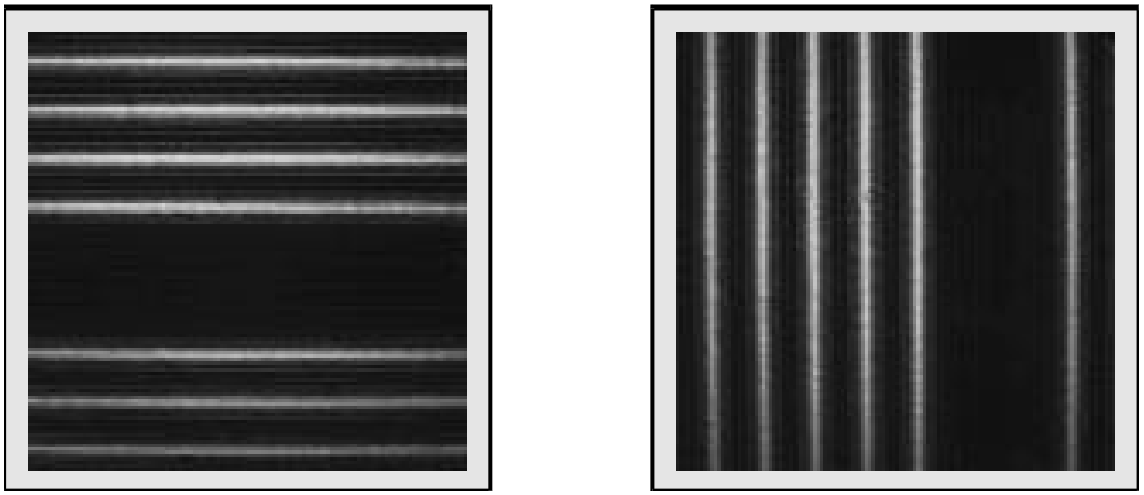

Fig. 6.2.2: First pair of ronchigrams: (a) Ruling lines along the X axis; (b) Ruling lines along the Y axis.

(a) (b)

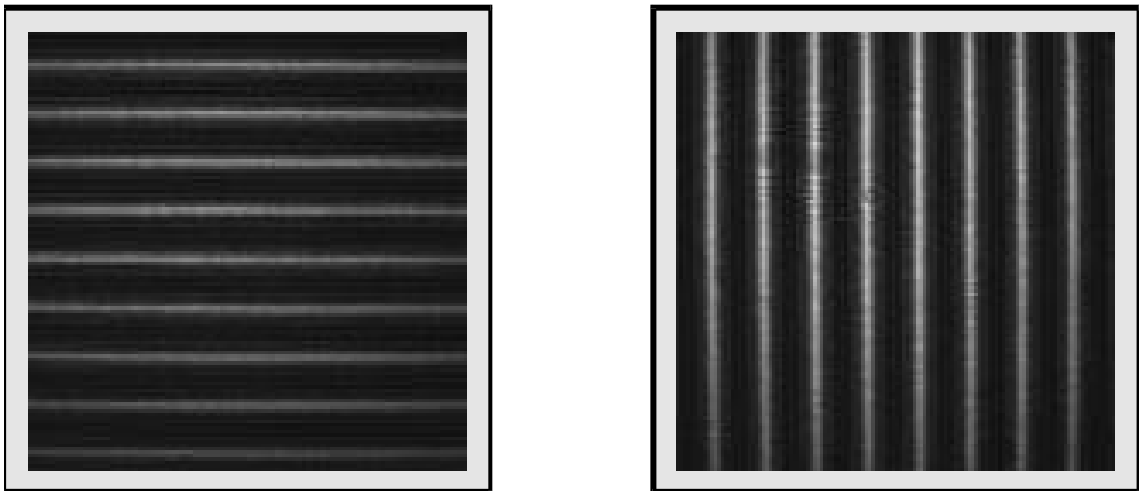

Fig. 6.2.2 shows the original ronchigrams obtained under the aforementioned experimental conditions. Their equivalence to those of Fig. 6.2.1 is obvious, the only difference being the presence of the two bright lines, which were hidden in the reference images. The number of bright lines in both ronchigrams need not be the same, as it depends on the position of the Ronchi ruling. Furthermore, in the displacements of the

ruling performed through microstepping procedures the number of bright lines present in each ronchigram at a given direction may not be constant.

The non-microstepped procedure needs only the pair of ronchigrams presented in Fig. 6.2.2. In the microstepped procedure this pair is used as the first of a series of ten pairs with 50.8μm displacements of the ruling between them along the X and Y axes. First, the complete series of ten ronchigrams with the ruling lines placed along the X axis is recorded, and then the ruling is tilted 90° using the stepper motor to register ten ronchigrams with the ruling lines along the Y axis. The process is fully automated so the user only needs to introduce a few experimental parameters before the complete set of data is acquired. A microstepped data recording process lasts about fifteen minutes. A non-microstepped measurement lasts two minutes, approximately, including the time taken to acquire the reference images. However, most of the time is used to position the ruling through the encoder motors, which could easily be improved by using more suitable motors to perform the ruling displacement.

Once the experimental measurements are obtained, the data processing procedures described in Section 4.2 may start. The initial data from the ronchigrams is first smoothed (Fig.6.2.3) and then binarized through a threshold operation (Fig.6.2.4). Once the data has been prepared, the reduction of the wide lines in the ronchigram to its central pixel yields the eroded ronchigrams (Fig.6.2.5). When microstepping procedures are applied, these data processing operations are performed on each ronchigram, giving a set of twenty smoothed, binarized and eroded ronchigrams.

Fig. 6.2.3: Smoothed ronchigrams: (a) Ruling lines along the X axis; (b) Ruling lines along the Y axis.

(a) (b)

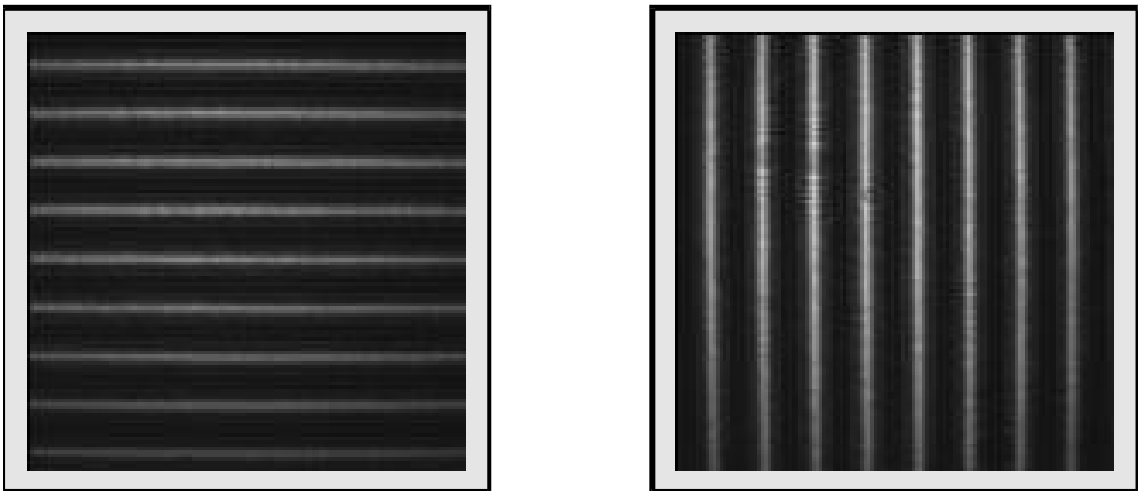

Fig. 6.2.4: Binarized ronchigrams: (a) Ruling lines along the X axis; (b) Ruling lines along the Y axis.

(a) (b)

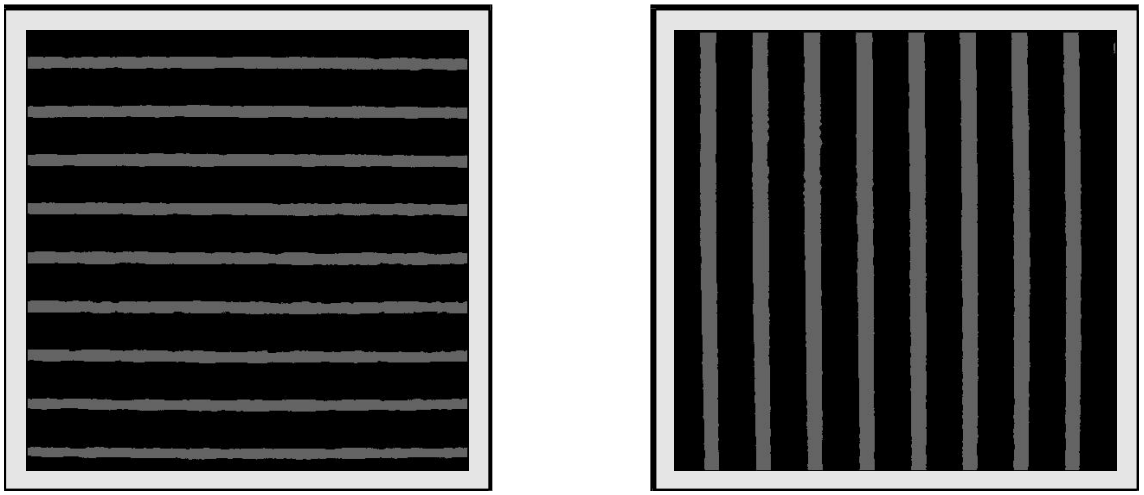

Fig. 6.2.5: Eroded ronchigrams: (a) Ruling lines along the X axis; (b) Ruling lines along the Y axis.

(a) (b)

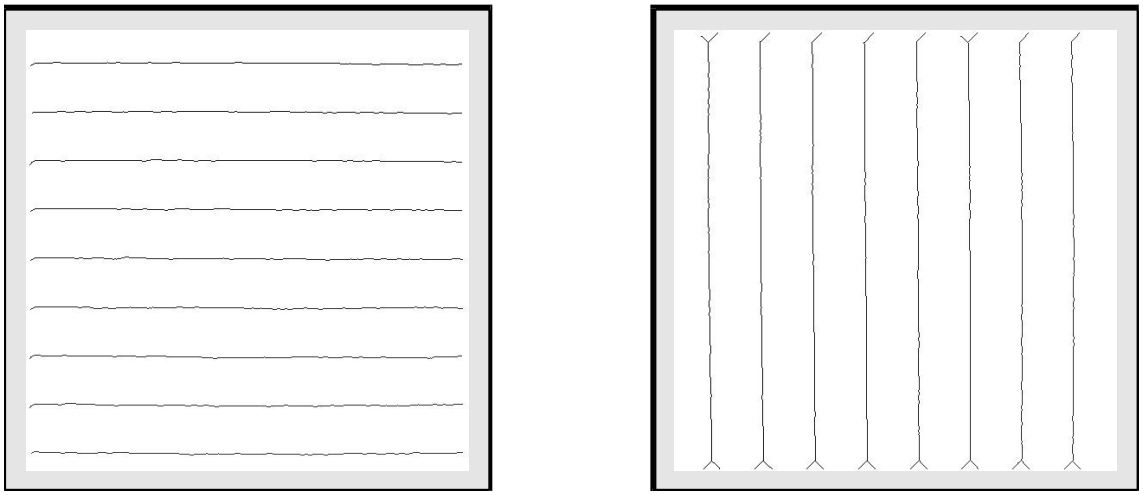

Fig. 6.2.6 gives the superposition of the original pair of ronchigrams with its corresponding eroded ronchigram. It may be seen how the eroding procedure reduces the wide bright fringes in the ronchigram to their central pixel row (or column). A pair of segments with a length of some pixels may be observed at each of the ends of the lines, which depart from the succession of central pixels of the bright wide line. This short segment is a consequence of the eroding procedure, which at the edge of each wide line starts eroding along both sides, until the coincidence in a single pixel of both segments shows they belong to a same wide line. Further algorithms intended to

remove the extra perpendicular lines that sometimes appear in the eroded ronchigrams may eradicate some of these short segments. Incidentally, as they only appear at the outer limits of the ronchigram, they will give rise to wrong sampled points only at the edge of the field and only if they intersect with any of the lines from the set of ronchigrams with perpendicular lines.

Fig. 6.2.6: (a) Superposition of original and eroded ronchigrams: (a) Ruling lines along the X axis; (b) Ruling lines along the Y axis.

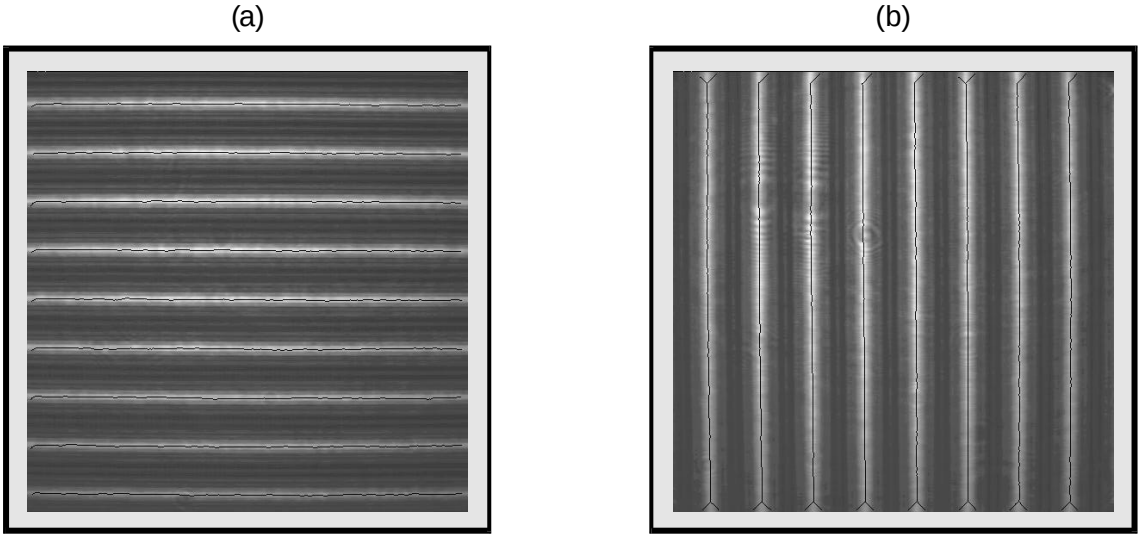

The eroded ronchigrams along the X and Y axes are then combined, as may be seen in Fig. 6.2.7. The intersection points of the eroded ronchigrams along the X and Y axes will determine the sampled points of the wavefront at the Ronchi ruling plane, as the slope of the wavefront along the X and Y axes (u,v) at the intersection points of the ronchigrams, with position (x_R,y_R), is known. Fig. 6.2.7a shows the result of the superposition step when microstepping was not used in the experiment; Fig. 6.2.7b shows the intersection points of the complete set of twenty ronchigrams obtained when applying microstepping procedures. Here, the benefits and drawbacks of microstepping procedures are shown: while the sampling of the surface has been greatly improved, as may be seen in the figure, the amount of information to process has increased by the same amount. Merely as an example, the number of sampling points increases from 74 to 7584 using microstepping procedures, making the size of the text file needed to save the (x_R,y_R,u,v) coordinates of each sampled point rise from 3Kb to 394Kb.

Fig. 6.2.7: Combination of eroded ronchigrams: (a) Without microstepping; (b) With microstepping.

(a) (b)

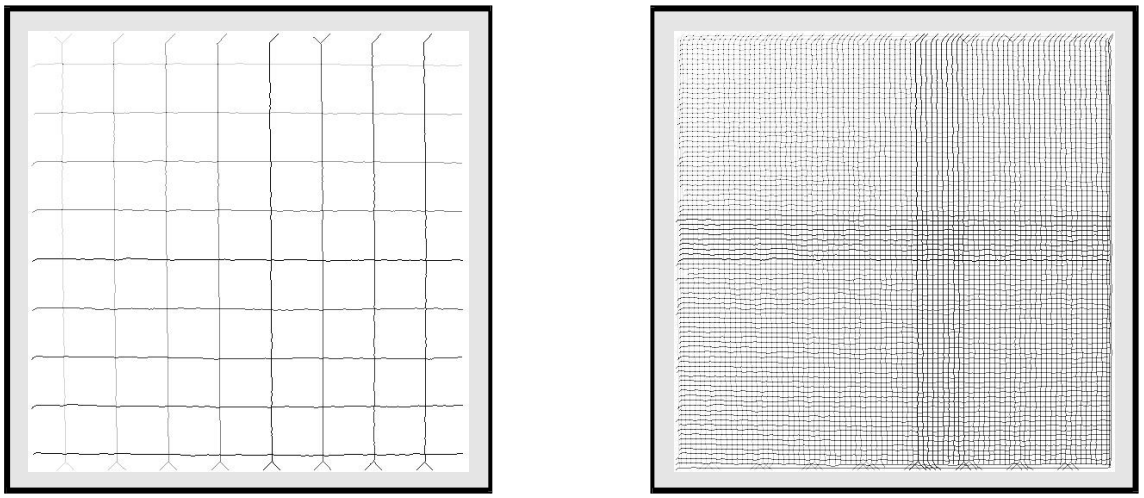

This set of position and slope data from the wavefront that we have extracted from the ronchigrams will start the following data processing steps. The data obtained is presented for the microstepped and non-microstepped measurements in Fig.6.2.8, where $y_R(x_R)$, $u(x_R)$ and $v(y_R)$ plots may be seen. Notice how the main difference between microstepped and non-microstepped data is the number of sampling points obtained.

The slopes of the $u(x_R)$ and $v(y_R)$ curves do not give the surface's radius of curvature, but that of the reflected wavefront when hitting the Ronchi ruling, if we assume this reflected wavefront is close to a spherical shape. It is stressed that this assumption is only needed in order to perform linear regression procedures on the $u(x_R)$ and $v(y_R)$ curves, but no assumption on the shape of the surface is needed in order to obtain topographic reconstructions of the measured wavefront. Here what we are displaying is the ability of our approach to the Ronchi test technique to make wavefront measurements, as a topographic reconstruction of the wavefront could easily be achieved from the measured data by taking steps very similar to the ones used in our surface integration procedures.

Getting back to the surface's radius of curvature, two-dimensional linear regression procedures yield the curvature of the wavefront at the Ronchi ruling, and an additional independent term which is an angular value related to misalignments and/or tilts of the sample surface relative to the incident wavefront. This independent term will be termed angular misalignment from now on.

Fig. 6.2.8: Measured data of the wavefront impinging on the Ronchi ruling: (a) $y_R(x_R)$ without microstepping; (b) $y_R(x_R)$ with microstepping; (c) $u(x_R)$ without microstepping; (d) $u(x_R)$ with microstepping; (e) $v(y_R)$ without microstepping; (f) $v(y_R)$ with microstepping